Heat Mass Transfer (2009) 45:1293–1302
DOI 10.1007/s00231-009-0507-8

ORIGINAL

Interaction of surface radiation with combined conduction and convection from a discretely heated L-corner

C. Gururaja Rao · D. Santhosh · P. Vijay Chandra

Received: 26 June 2008 / Accepted: 26 March 2009 / Published online: 10 July 2009

Abstract Prominent results pertaining to the problem of multi-mode heat transfer from an L-corner equipped with three identical flush-mounted discrete heat sources in its left leg are given here. The heat generated in the heat sources is conducted along the two legs of the device before being dissipated by combined convection and radiation into air that is considered to be the cooling agent. The governing equations for temperature distribution along the L-corner are obtained by making appropriate energy balance between the heat generated, conducted, convected and radiated. The non-linear partial differential equations thus obtained are converted into algebraic form using a finite-difference formulation. The resulting equations are solved simultaneously by Gauss–Seidel iterative solver. A computer code is specifically written to solve the problem. The computational domain is discretised using 101 grids along the left leg, with 15 grids taken per heat source, and 21 grids along the bottom leg. The effects of surface emissivity, convection heat transfer coefficient, thermal conductivity and aspect ratio on local temperature distribution, peak device temperature and relative contributions of convection and radiation to heat dissipation from the L-corner are studied in detail. The point that one cannot overlook radiation in problems of this class has been clearly elucidated.

List of symbols

A	Aspect ratio, L/W
F_{kl}	View factor of a given element k with reference to another element l of the L-corner
h	Convection heat transfer coefficient (W/m^2 K)
$J_h(i)$	Radiosity of an element i of the bottom leg of the L-corner (W/m^2)
$J_v(k)$	Radiosity of an element k of the left leg of the L-corner (W/m^2)
k_s	Thermal conductivity of the material of the L-corner (W/m K)
L	Height of the L-corner (m)
L_h	Height of each of the discrete heat sources of the L-corner (m)
M	Number of nodes along the bottom leg of the L-corner
N	Number of nodes along the left leg of the L-corner
N_1	Node number at the interface between the first heat source and the non-heat source portion along the left leg of the L-corner
q_v	Volumetric heat generation in each of the three heat sources (W/m^3)
t	Thickness of the L-corner (m)
T_∞	Ambient air temperature (K)
$T_h(i)$	Temperature of an element i of the bottom leg of the L-corner (K)
T_{max}	Peak device temperature (K)
$T_v(k)$	Temperature of an element k of the left leg of the L-corner (K)
W	Width of the L-corner (m)
x	Co-ordinate direction along the left leg (m)
y	Co-ordinate direction along the bottom leg (m)

Greek symbols

α	Absorptivity of the L-corner
Δx_{hs}	Length of an element in the heat source portion along the left leg (m)
Δx_{nhs}	Length of an element in the non-heat source portion along the left leg (m)

C. Gururaja Rao (✉) · D. Santhosh · P. Vijay Chandra
Department of Mechanical Engineering, National Institute of Technology, Warangal, Andhra Pradesh 506004, India
e-mail: cgr_gcr@yahoo.co.in

Δy_{nhs} Length of an element in the non-heat source portion along the bottom leg (m)
ε Surface emissivity of the L-corner
σ Stefan–Boltzmann constant (5.6697×10^{-8} W/m^2 K^4)

Subscripts

cond, x, in Conduction heat transfer into an element of the left leg of the L-corner
cond, x, out Conduction heat transfer out of an element of the left leg of the L-corner
cond, y, in Conduction heat transfer into an element of the bottom leg of the L-corner
cond, y, out Conduction heat transfer out of an element of the bottom leg of the L-corner
conv Convection heat transfer from an element
i Any arbitrary element along the bottom leg
k Any arbitrary element along the left leg
rad Heat transfer by surface radiation from an element

1 Introduction

Several researchers have come out with analytical, numerical and experimental studies on the problems of multi-mode heat transfer from various geometries with varying complexities. Zinnes [1] is one of those initial researchers presenting his results of the problem of combined conduction and laminar natural convection from a vertical flat plate of finite thickness with an arbitrary heating distribution over its surface. Others following him include Tewari and Jaluria [2], Merkin and Pop [3], Cole [4], Hossain and Takhar [5]. With regard to multi-mode heat transfer studies that incorporate mixed convection coupled with conduction and surface radiation, Gururaja Rao et al. [6] presented results of conjugate mixed convection with radiation from a vertical plate equipped with a discrete heat source. Here, they solved the problem without the conventional boundary layer approximations. Subsequently, the same authors [7, 8] solved the conjugate heat transfer problems pertaining to the geometry of a vertical channel with, respectively, uniform wall heat generation and discrete wall heat generation. Gururaja Rao [9] studied the effect of traversing the discrete heat source along a vertical electronic board subjected to buoyancy-aided mixed convection with conduction and radiation. Gururaja Rao et al. [10] solved, numerically, the problem of multi-mode heat transfer from a square shaped electronic device with multiple discrete heat sources. Gururaja Rao et al. [11] presented the results of their numerical probe into conjugate convection with radiation from an open cavity with a flush-mounted discrete heat source. Very recently, Sawant and Gururaja Rao [12] furnished the findings of their studies on conjugate mixed convection with surface radiation from a vertical electronic board with multiple discrete heat sources.

The review of the literature, a brief summary of which is provided above, indicates that enough information is not available about the interplay between the three modes of heat transfer for the geometry of an L-corner possessing discrete heat sources in its legs. On account of this, a numerical simulation of interaction of radiation with conjugate convection from the above geometry is attempted in the present paper. In addition to bringing out the role of radiation in the problem, the effects of various other parameters, like convection heat transfer coefficient, thermal conductivity and aspect ratio, have also been brought out.

2 Problem definition and mathematical formulation

Figure 1 shows the schematic of the problem geometry chosen for study. It consists of an L-corner of height L, width W and thickness t. There are three identical flush-mounted discrete heat sources, each of height L_h and thickness t, provided along the left leg of the L-corner. The above heat sources are equi-spaced, with the first at the bottom of the leg, the second at the centre and the third at the top of the leg. The left and the top surfaces of the left leg and the bottom and the right surfaces of the bottom leg are adiabatic. The heat generated in the discrete heat sources is first conducted along the two legs of the L-corner, before getting subsequently dissipated from the right surface of the left leg and the top surface of the bottom leg into ambient air by combined modes of convection and radiation. Here, the cooling agent (air) is considered to be radiatively transparent. Assuming $t \ll L$ (or W), the transverse conduction in the two legs of the L-corner is ignored.

The governing equations for the temperature distribution along the L-corner are obtained by appropriate energy balance between the heat generated, conducted, convected and radiated. For example, energy balance on a typical element pertaining to the interior of each of the three heat sources along the left leg gives:

$$q_{x,\mathrm{cond,in}} + q_v(\Delta x_{hs} t) = q_{x,\mathrm{cond,out}} + q_{conv} + q_{rad} \quad (1)$$

On substituting relevant expressions for various terms in the above, one gets

$$q_v(\Delta x_{hs} t) = \left(\frac{\partial}{\partial x} q_{x,\mathrm{cond,in}}\right)\Delta x_{hs} + h(\Delta x_{hs})[T_v(k) - T_\infty] + \frac{\varepsilon}{1-\varepsilon}\left[\sigma T_v^4(k) - J_v(k)\right](\Delta x_{hs}) \quad (2)$$

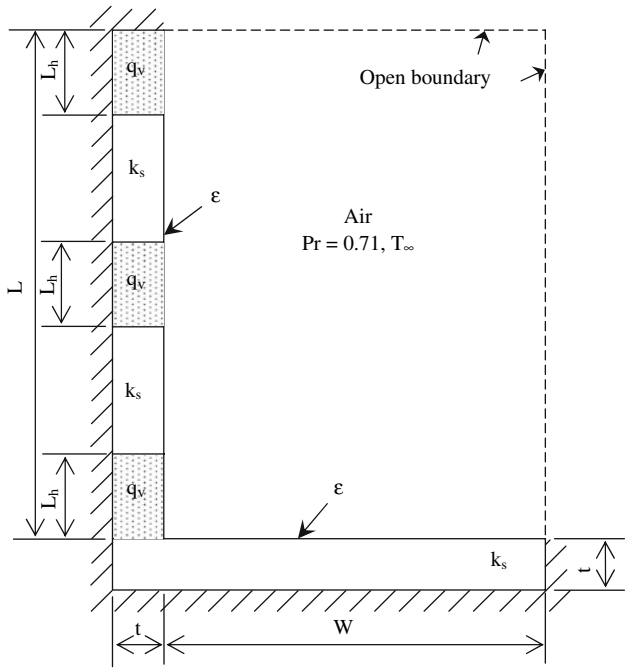

Fig. 1 Schematic of the problem geometry chosen in the present study

Here $T_v(k)$ denotes the absolute temperature of the element in question, while $J_v(k)$ signifies the radiosity of the same element given as

$$J_v(k) = \varepsilon\sigma T_v^4(k) + (1-\varepsilon)\sum_{l=1}^{n} F_{kl}J_l \tag{3}$$

where F_{kl} indicates the view factor of the element under consideration with reference to each of the n elements of the complete enclosure. J_l stands for the radiosity of any given element of the enclosure. It is to be noted that the enclosure here comprises the two legs of the L-corner and two open (or free) boundaries, which are assumed to be black ($\varepsilon = 1$) at the temperature equal to that of the ambient (T_∞). The updated governing equation, after some simplification, looks as:

$$\frac{\partial^2 T_v(k)}{\partial x^2} - \frac{h}{k_s t}[T_v(k) - T_\infty] - \frac{\varepsilon}{k_s t(1-\varepsilon)}\left[\sigma T_v^4(k) - J_v(k)\right] + \frac{q_v}{k_s} = 0 \tag{4}$$

With regard to the temperature at the interface between a given heat source and the non-heat source portion of the left leg, Fig. 1 shows that there are four elements of that kind. Considering one such element that is present at the interface between the bottom most heat source and the left leg, and making energy balance on it,

$$q_{x,\mathrm{cond,in}} + q_v\left[\left(\frac{\Delta x_{hs}}{2}\right)t\right] = q_{x,\mathrm{cond,out}} + q_{conv} + q_{rad} \tag{5}$$

After appropriately invoking the concerned expressions for various terms of the above equation, the governing equation for the temperature of the element under consideration comes out to be

$$\frac{\partial^2 T_v(N_1)}{\partial x^2} + \frac{q_v}{k_s}\left(\frac{\Delta x_{hs}}{\Delta x_{hs} + \Delta x_{nhs}}\right) - \frac{h}{k_s t}[T_v(N_1) - T_\infty] - \frac{\varepsilon}{(1-\varepsilon)k_s t}\left[\sigma T_v^4(N_1) - J_v(N_1)\right] = 0 \tag{6}$$

The temperature corresponding to the left bottom corner of the device is obtained by pertinent energy balance that leads to:

$$\frac{\partial T_v(1)}{\partial x} + \frac{\partial T_v(1)}{\partial y} + \frac{q_v}{k_s}\left(\frac{\Delta x_{hs}}{2}\right) - \frac{h}{k_s t}\left(\frac{\Delta x_{hs} + \Delta y_{nhs}}{2}\right)[T_v(1) - T_\infty] - \frac{\varepsilon}{(1-\varepsilon)k_s t}\left(\frac{\Delta x_{hs} + \Delta y_{nhs}}{2}\right)\left[\sigma T_v^4(1) - J_v(1)\right] = 0 \tag{7}$$

The governing equation for temperature distribution along the bottom leg other than the right adiabatic end is obtained using similar procedure as

$$\frac{\partial^2 T_h(i)}{\partial y^2} - \frac{h}{k_s t}[T_h(i) - T_\infty] - \frac{\varepsilon}{(1-\varepsilon)k_s t}\left[\sigma T_h^4(i) - J_h(i)\right] = 0 \tag{8}$$

In the above equation, $T_h(i)$ and $J_h(i)$ would mean the same as the corresponding terms $T_v(k)$ and $J_v(k)$ in Eq. (2).

As can be seen from Fig. 1 there are two adiabatic ends for the device. Considering the adiabatic end belonging to the left leg of the L-corner and applying the same mathematical treatment as above, the concerned governing equation would be

$$\frac{\partial T_v(N)}{\partial x} - \frac{q_v}{k_s}\left(\frac{\Delta x_{hs}}{2}\right) + \frac{h}{k_s t}\left(\frac{\Delta x_{hs}}{2}\right)[T_v(N) - T_\infty] + \frac{\varepsilon}{(1-\varepsilon)}\left(\frac{\Delta x_{hs}}{2k_s t}\right)\left[\sigma T_v^4(N) - J_v(N)\right] = 0 \tag{9}$$

The equations for temperature distribution for the rest of the elements of the L-corner that include the non-heat source portions of the left leg and the adiabatic end of the bottom leg, are obtained in a similar manner.

3 Method of solution and range of parameters

The governing equations for temperature distribution along the L-corner obtained as above are non-linear partial differential equations. These equations are first converted into algebraic form using a finite-difference formulation. The

resulting finite-difference equations are solved simultaneously using Gauss–Seidel iterative technique. The discretisation of the computational domain is made such that there are finer grids wherever heat sources are present in the L-corner, while coarser grids would suffice in the rest of the device. The optimum grid system for the study is obtained through a rigorous grid sensitivity analysis, the results of which follow in an ensuing section. Full relaxation (relaxation parameter = 1) has been used on temperature during iterations, while a stringent convergence criterion of 10^{-8} is used to terminate the iterations. A computer code is written specifically for solving the present problem.

The ranges of different governing parameters for the present study are decided based on some of the earlier works of this kind reported in the literature. The range for surface emissivity (ε) is taken to be 0.05–0.85, with the lower limiting value 0.05 signifying a poor emitter (e.g., a highly polished aluminum sheet). The upper limit ($\varepsilon = 0.85$) pertains to a good emitter (like black paint). For thermal conductivity (k_s), all the studies make use of the range 0.25–1 W/m K. The above range for k_s is in agreement with Pieterson and Ortega [13], which reports the material for electronic boards to be typically Mylar coated epoxy glass having a thermal conductivity of 0.26 W/m K. For convection heat transfer coefficient (h), the range is taken to be 5–100 W/m^2 K, with $h = 5$ W/m^2 K implying an asymptotic free convection limit and $h = 100$ W/m^2 K signifying an asymptotic forced convection limit. The appropriate range for volumetric heat generation in each discrete heat source (q_v) is fixed keeping in mind the maximum temperature typically permitted for electronic devices ($\approx$150°C). In addition to the above parameters, for some of the studies in the present work, the aspect ratio ($A = L/W$) too is varied keeping the height of the left leg of the L-corner (L) fixed at 20 cm.

4 Results of the study

4.1 Grid sensitivity analysis

In order to arrive at the optimum grid size for discretising the computational domain, a grid convergence test is performed in three phases. For all the phases of the test, a fixed set of input parameters, comprising $L = 20$ cm, $t = 1.5$ mm, $L_h = 2.5$ cm, $T_\infty = 25$°C, $A = 4$, $k_s = 0.25$ W/m K, $h = 5$ W/m^2 K, $\varepsilon = 0.45$ and $q_v = 5 \times 10^5$ W/m^3, has been taken. In the first phase of the study, the number of grids along the bottom leg (M) is taken to be 31 and the number of grids per heat source is taken to be 10, while the number of grids along the left leg (N) is varied. Table 1 shows the results of the above study. It can be seen that, the peak device temperature (T_{max}) changes by 0.0019% as N increases from 91 to 101. A further increase of N from 101 to 111 is changing T_{max} only by 0.0009%. Further, energy balance check also works out satisfactorily for all the three values of N (i.e., 91, 101 and 111). In view of the above, the value of N is frozen on 101 for the whole study. The second phase of the grid study assumes the number of grids along each heat source to be 10, while the value of N is taken to be 101 owing to the results of the first phase. The value of M is varied here. Table 2 shows the pertinent results. It is noticed that T_{max} changes by 0.0016% as M increases from 11 to 21. A further increase of M to 31 is changing T_{max} only by 0.0003%. Further, the energy balance check also supports the value of $M = 21$. In view of this, a value of $M = 21$ is considered apt for the present problem. In the third phase of the grid sensitivity test, whose results are shown in Table 3, M and N are kept fixed at 21 and 101 as a consequence of the earlier two phases. The number of grids along each heat source is varied. It can be seen that the change in T_{max} is by 0.07% as the number of elements per heat source is increased from 10 to 15. The value of T_{max} changes only by a further 0.04% as each heat source is provided with 20 elements in

Table 1 First phase of grid sensitivity analysis with varying values of N ($M = 31$ and number of elements per heat source = 10)

S. no.	N	T_{max} (°C)	Percentage change (abs.)	Check for energy balance (abs.) (%)
1	51	106.864	–	0.1031
2	61	106.893	0.0271	0.1015
3	71	106.904	0.0103	0.1009
4	81	106.909	0.0047	0.1006
5	91	106.912	0.0028	0.1004
6	101	106.914	0.0019	0.1003
7	111	106.915	0.0009	0.1002

Table 2 Second phase of grid sensitivity analysis with varying values of M ($N = 101$ and number of elements per heat source = 10)

S. no.	M	T_{max} (°C)	Percentage change (abs.)	Check for energy balance (abs.) (%)
1	11	106.9160	–	0.3149
2	21	106.9143	0.0016	0.0513
3	31	106.9140	0.0003	0.1003

Table 3 Third phase of grid sensitivity analysis with varying number of elements along heat source ($M = 21$ and $N = 101$)

S. no.	No. of elements per heat source	T_{max} (°C)	Percentage change (abs.)	Check for energy balance (abs.) (%)
1	10	106.9143	–	0.0513
2	15	106.8402	0.0693	0.1369
3	20	106.7971	0.0404	0.1988

place of 15. The above results thus confirm the optimum value for the number of elements per heat source to be 15. In conclusion, the grid convergence test performed as above confirms that $M = 21, N = 101$ and the number of grids per heat source $= 15$ provide the most appropriate grid system for the entire study.

4.2 Study of local temperature distribution with reference to various parameters

In order to study the nature of variation of local temperature distribution along the L-corner with surface emissivity (ε) results are obtained for $q_v = 5 \times 10^5$ W/m^3, $A = 4$, $k_s = 0.25$ W/m K and $h = 5$ W/m^2 K. Three different values of ε are chosen, viz., 0.05, 0.45 and 0.85. Figure 2a and b show the results for the left leg and the bottom leg of the L-corner, respectively. With regard to the left leg, as depicted by Fig. 2a, for a given emissivity, the temperature increases sharply to a local maximum near the midpoint of the bottommost heat source. From here the temperature decreases again till a local minimum is reached, with an increase in temperature again taking place from there. This continues until a second local maximum is noticed at around the center of the left leg. From here, the temperature again decreases to a second local minimum, before shooting up yet again with the maximum temperature attained at the adiabatic top end of the left leg of the L-corner. To summarize, there are three local peaks along the left leg with the last one noticed at the top adiabatic end being the maximum, while the peaks in the bottommost and the central heat sources of the left leg taking the next two places. For all the three values of surface emissivity chosen the trend of the local left leg temperature is found to be the same. However, at a given location, the temperature decreases as ε increases, appreciably between $\varepsilon = 0.05$ and 0.45 and less pronouncedly between $\varepsilon = 0.45$ and 0.85. For example, the second local peak temperature along the left leg drops down by 25.51% as ε increases from 0.05 to 0.45, while it further drops down by 15.91% due to a subsequent rise in ε to 0.85.

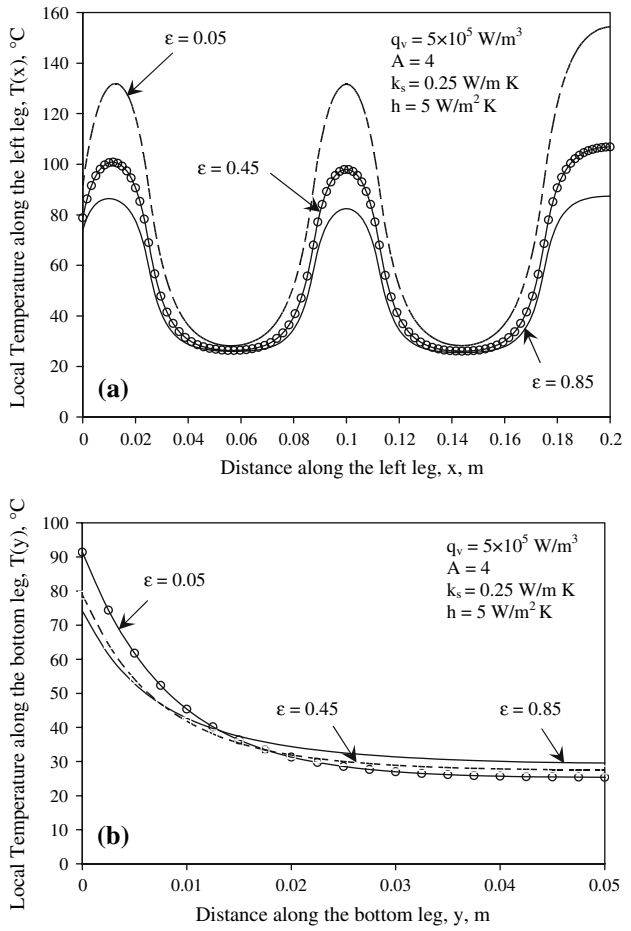

Fig. 2 Local temperature distribution along the **a** left leg and **b** bottom leg of the L-corner for different surface emissivities

The bottom leg of the L-corner merely conducts the heat generated in the heat sources of the left leg and subsequently dissipates it by convection and radiation to the ambient. It also interacts with the left leg through radiation. Figure 2b indicates that the temperature along the bottom leg shows a monotonic decrease as one moves from the left end to the right end of it. However, the three curves pertaining to the three different values of emissivity cross each other. For example, the curve pertaining to $\varepsilon = 0.45$ is crossing the one belonging to $\varepsilon = 0.05$ ahead of the central portion of the bottom leg. Due to this the local temperature of the bottom leg for $\varepsilon = 0.45$ would be greater than that for $\varepsilon = 0.05$ beyond the point of crossover. The reason for the above could be due the increased absorption of irradiation received from the left leg owing to increase in absorptivity, α [that equals emissivity (ε) owing to gray body assumption] from 0.05 to 0.45. Similar trends are noticed with regard to crossing of the other sets of curves too.

In order to investigate the nature of variation of the local temperature distribution along the L-corner in the entire regime of convection considered, Fig. 3a and b are plotted for the case with $q_v = 5 \times 10^5$ W/m^3, $A = 4$, $k_s = 0.25$ W/m K and $\varepsilon = 0.45$. Four different values of convection heat transfer coefficient (h) are chosen as shown in the figures with $h = 5$ W/m^2 K and $h = 100$ W/m^2 K indicating the limiting cases of free and forced convection. A look at Fig. 3a reveals that the general trend of the left leg local temperature profile is the same as that exhibited in Fig. 2a. There are three local maxima here also with the third one noticed at the top adiabatic end of the left leg turning out to be the peak device temperature. The figure further shows that, though there is an expected decrement in local temperature with increasing h, the convection heat transfer coefficient shows a significant effect between 5 and 25 W/m^2 K, while its effect peters

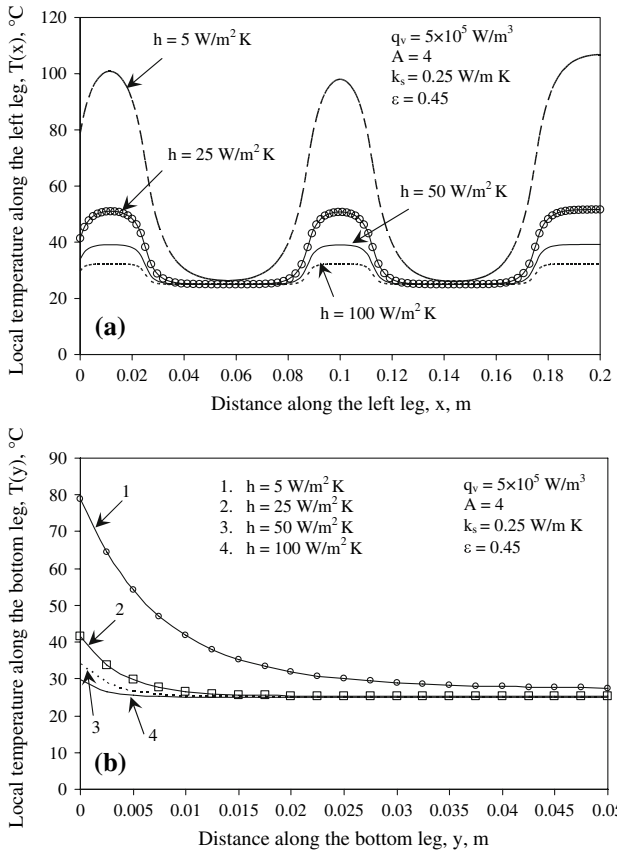

Fig. 3 Local temperature distribution along the **a** left leg and **b** bottom leg of the L-corner in various regimes of convection

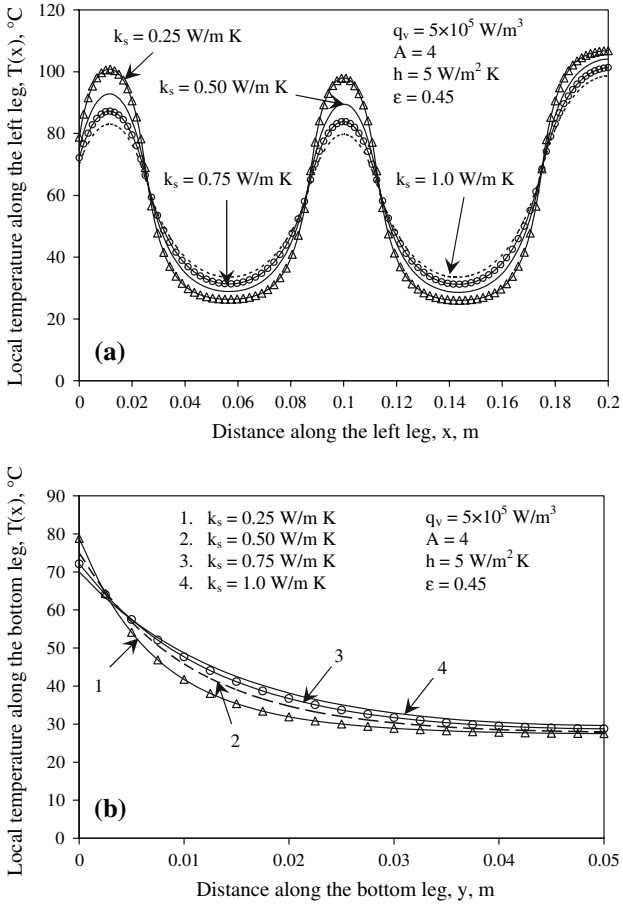

Fig. 4 Variation of local temperature along the **a** left leg and **b** bottom leg for different thermal conductivities of the L-corner

down as its value increases further from 25 to 100 W/m^2 K. In the present example, the central peak temperature of the left leg is found to be decreasing by 48.12% as h increases from 5 to 25 W/m^2 K. In contrast, the same local temperature decreases by meagre 32.28% due to a further increase of h from 25 to 100 W/m^2 K. Coming to the bottom leg, Fig. 3b shows that there is a comparatively sharper drop in the local temperature in the initial portion of the bottom leg spanning over 20% of its length. From there, the local temperature diminishes only notionally up to the adiabatic end of the bottom leg, where expectedly there is a local minimum. Like with the left leg, the bottom leg too has its temperature greatly influenced by h between 5 and 25 W/m^2 K when compared to the remaining range of h considered. The present study thus tacitly hints that $h = 25$ W/m^2 K is an optimum value of convection heat transfer coefficient for the given problem with other parameters held fixed as given above.

Figure 4 describes the effect of the thermal conductivity (k_s) of the L-corner on the local temperature distribution for a given set of parameters, namely $q_v = 5 \times 10^5$ W m^{-3}, $A = 4$, $h = 5$ W/m^2 K and $\varepsilon = 0.45$. Four values of k_s [0.25, 0.50, 0.75 and 1 W/m K] have been chosen. Figure 4a pertains to the left leg of the L-corner while Fig. 4b belongs to its bottom leg. Figure 4a indicates that the nature of the left leg temperature profile for a given k_s is similar to that noticed in Figs. 2a and 3a. However, as the thermal conductivity increases, though there is an expected drop in the device temperature in the three heat sources, the trend is completely reversed in the non-heat source portions of the left leg. This is attributed to the fact that the non-heat source potions are passive simply percolating the heat generated in the heat sources in the left leg. Due to this, increasing conductivity obviously means diminishing temperature gradient. In the present example, in the central heat source portion of the left leg, the local peak temperature is decreasing by 18.66% as k_s increases from 0.25 to 1 W/m K. In contrast, if one considers the non-heat source portion between the central and the topmost heat sources of the leg, owing to the reasons mentioned above, the local minimum in the portion concerned is increasing by 28.64% between the same limits of k_s as above. As far as the bottom leg is concerned, in general, the temperature variation resembles that along a fin with the maximum noticed at the left bottom corner of the device. Again here, since

the values of h and ε are the same for all the curves pertaining to the four values of thermal conductivity taken, barring some initial distance from the left end of the bottom leg, the local temperature increases with increasing k_s. The above again is due to the diminishing temperature gradient with increasing thermal conductivity of the device. In the present case, at midway along the bottom leg, the local temperature increases from 30.02 to 35.09°C as k_s increases from 0.25 to 1 W/m K. Note that the temperature rise is only notional due to the fact that the thermal conductivities chosen are all very small differing only by 0.25 W/m K.

In order to study the contrast, if any, between the local temperature profiles along the left leg of the L-corner in different possible situations, viz., (1) all three heat sources present, (2) only the bottom most heat source present, (3) only the central heat source present and (4) only the top most heat source present, Fig. 5 has been drawn. The above is done for a fixed input of $q_v = 5 \times 10^5$ W/m^3, $A = 4$, $k_s = 0.25$ W/m K, $h = 5$ W/m^2 K and $\varepsilon = 0.05$. The figure shows that the temperature profile for case (1), which is like any of the situations discussed in Figs. 2, 3 and 4, looks much like in the earlier three figures. When once only one of the three heat sources is considered present with the other two absent, as done in cases (2), (3) and (4), the temperature profiles assume different shapes. In case (2), where only the heat source at the bottom corner is present, the local left leg temperature after sharply increasing to a maximum decreases equally sharply to a very low value [$\approx T_\infty$] and remains asymptotic thereafter. In case (3), where only the central heat source alone is present, the left leg temperature remains almost at the fluid temperature (T_∞) up to about one quarter length of the left leg. From there, the temperature rises sharply, reaches its peak at the midpoint of the left leg and decreases once again. The top-half portion of the temperature profile that follows now looks like a mirror image to that in the bottom half of the leg. With regard to case (4) that considers the presence of only the topmost heat source, the temperature of the left leg remains almost at the temperature of the cooling agent (T_∞) up till three quarter length of the left leg. Only from here, the temperature shoots up abruptly and reaches its peak at the top adiabatic end of the left leg. The figure further reveals that, if one were to use a single heat source in the L-corner, the best possible position for it would be the centre of the left leg. The next preferable position would be the bottommost position and the topmost position is the least preferable option. In the present example, the peak temperatures attained in cases (2), (3) and (4) are 131.71, 131.41 and 154.35°C, respectively. As can be seen, though there is hardly anything to choose between the options (2) and (3), still option (3) is the best. When one compares options (2) and (3) with (4), there will be an undue load on the cooling system with option (4) owing to 17.46% rise in T_{max} compared to option (3). Incidentally, even when one uses all the three heat sources in the left leg [option (1)], the maximum device temperature is turning out to be almost the same as that in the case where only the topmost heat source is present. This serves to say that, in the case where all the heat sources are present the conduction through the non-heat source potions is just adequate in keeping the device temperature under check on par with the worst possible case where singular topmost heat source is present.

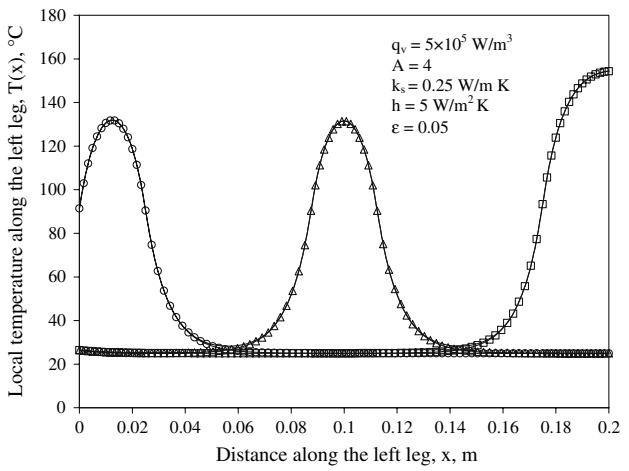

Fig. 5 Local temperature distribution along the left leg with all the heat sources and with one heat source each taken at a time

4.3 Variation of peak L-corner temperature with other parameters

A study of variation of the maximum temperature of the L-corner (T_{max}) with surface emissivity in the entire regime of convection considered has been made for an input comprising $q_v = 5 \times 10^5$ W/m^3, $A = 4$ and $k_s = 0.25$ W/m K. The results are as shown in Fig. 6. It can be seen from the figure that, for a given regime of convection (given value of h), T_{max} decreases with increasing ε on account of increased share from radiation in dissipating the heat from the L-corner. The above effect of ε is distinctly noticed for smaller values of h (<25 W/m^2 K). This is because, in the regime of convection pertaining to the above range, convection is predominantly out of buoyancy and thus is only to a smaller extent, which enables radiation to dominate in surface heat dissipation. In contrary to the above, with larger values of h taken, forced convection creeps in and dominates radiation no matter what the value of ε chosen is. Thus, one can see only a notional drop in T_{max} with increasing ε here (see curves 3, 4 and 5). The figure also implicitly shows that, for a given ε, one can control the peak device temperature by expending more pumping power and thus operating with

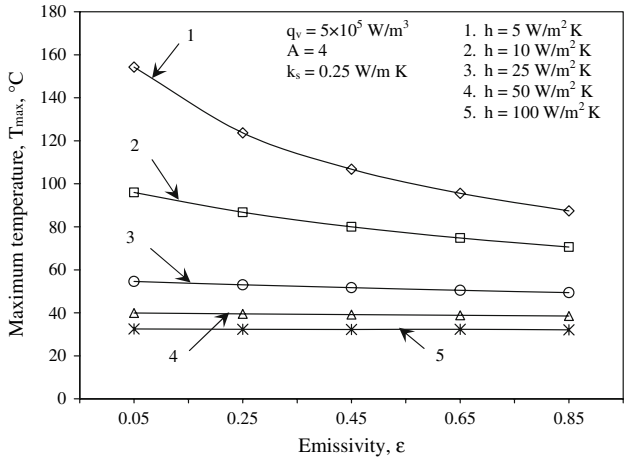

Fig. 6 Variation of maximum temperature of the L-corner with surface emissivity in various regimes of convection

increased values of h. To quantify the observations made above, in the present study, T_{max} drops down by 43.39% with ε increasing from 0.05 to 0.85, for $h = 5$ W/m^2 K. On the other hand, for $h = 100$ W/m^2 K, T_{max} comes down by a mere 1.08% as a result of the same increment in ε. Further, keeping ε fixed at a very low value of 0.05, a drop of 78.96% in T_{max} can be obtained by changing the flow regime from $h = 5$ to 100 W/m^2 K.

To bring out the interplay between conduction along the L-corner and convection from its surface in influencing T_{max}, a family of curves has been drawn as shown in Fig. 7. Four typical values of thermal conductivity (k_s), viz., 0.25, 0.5, 0.75 and 1 W/m K, are chosen, while three values of h (5, 10 and 25 W/m^2 K) are selected for study. The remaining input chosen for the study is fixed as shown in the figure. It may be seen that, for a given k_s, there is a considerable decrease in T_{max} with increasing value of h. However, the degree of decrement in T_{max} with increasing k_s for a given h is not substantial. The above may be attributed to the fact that, for a given k_s, by increasing h from 5 to 25 W/m^2 K, one is transiting from an asymptotic free convection limit to an asymptotic forced convection limit. This brings about a substantiative drop in T_{max}. However, since the values of k_s chosen for the study are very small, the activity of conduction is not picking up very much even when k_s is increased from 0.25 to 1 W/m K, for a given h. In the present example, for $k_s = 0.25$ W/m K, T_{max} is seen to be dropping down by as much as 45.93% with h rising from 5 to 25 W/m^2 K. In contrast, for $h = 5$ W/m^2 K, T_{max} is decreasing only by 4.26% as k_s is increased from 0.25 to 1 W/m K.

Figure 8 explains the results of the study made on the interaction of internal conduction along the L-corner with radiation from its surface in influencing the maximum device temperature. This is done taking into account four typical values of k_s (0.25, 0.5, 0.75 and 1 W/m K) and three different values of ε (0.05, 0.45 and 0.85) keeping the values of q_v, A and h fixed at 5×10^5 W/m^3, 6 and 5 W/m^2 K, respectively, for the whole study. For a given surface emissivity, T_{max} decreases with increasing k_s on account of increase in diffusion of heat through the L-corner. However, thermal conductivity is showing a marked effect on T_{max} for a given ε only towards smaller values of ε. For larger values of ε, radiation overrides conduction specifically because of lower values of k_s chosen for study. Due to the above reason, the decrease in T_{max} is quite nominal for ε greater than 0.45 with other parameters held fixed. To substantiate the above quantitatively, calculations made from Fig. 8 show that T_{max} is decreasing by 13.45 and 5.25%, respectively, for $\varepsilon = 0.05$ and $\varepsilon = 0.85$, as k_s rises from 0.25 to 1 W/m K. The figure also shows that, for a given k_s, changing the surface of the L-corner from one with $\varepsilon = 0.05$ to that with $\varepsilon = 0.45$ brings a greater drop in T_{max} compared to changing ε to 0.85 from 0.45. In the current example, for

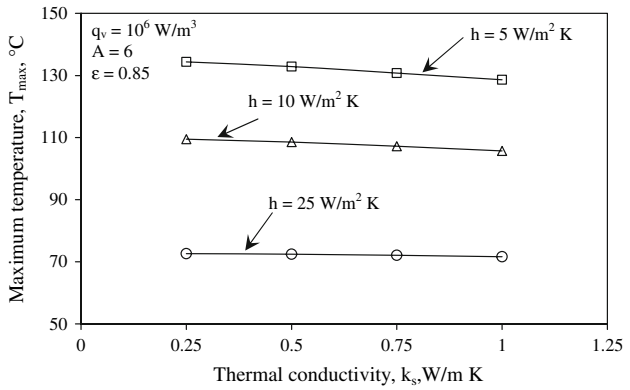

Fig. 7 Variation of maximum temperature of the L-corner with thermal conductivity in different regimes of convection

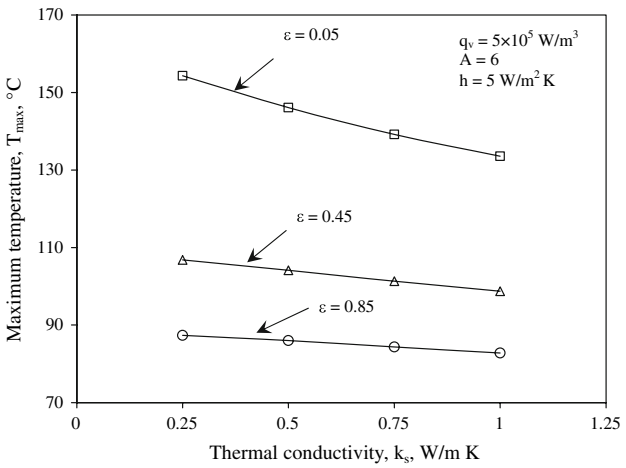

Fig. 8 Variation of maximum temperature of the L-corner with thermal conductivity for three typical surface emissivities

$k_s = 0.5$ W/m K, T_{max} is coming down by 28.73% as ε increases from 0.05 to 0.45. Against the above, the drop in T_{max} is only by 17.42% on increasing ε to 0.85 from 0.45 holding k_s fixed at 0.5 W/m K.

4.4 Contributory roles played by convection and radiation in heat dissipation

The delineation of convection and radiation in heat dissipation from the L-corner in various regimes of convection is studied as shown in Fig. 9. The probe is made for a fixed input of q_v, A and k_s as shown in the figure. Five typical values of ε and three different values of h are considered in the study as shown. The first interesting feature noticeable from the figure is that, for $h = 5$ W/m^2 K (asymptotic free convection limit), the relative contribution of convection in driving out the heat from the L-corner decreases continuously as ε increases from 0.05 to 0.85. A mirror image increase in the percentage share by radiation is seen between the same limiting values of ε. The above two curves belonging to convection and radiation cross each other for $\varepsilon \approx 0.774$, where convection and radiation take an identical share in heat dissipation, with radiation overpowering convection there after. Though not as pronounced as above, a similar kind of trend is observed in the roles played by convection and radiation towards higher values of h also. These results caution the designer not to overlook radiation in any of the regimes of convection due to the fact that it contributes about 15.38% to heat dissipation even for $h = 25$ W/m^2 K, which generally is an asymptotic forced convection limit, when $\varepsilon = 0.85$.

4.5 Effect of aspect ratio on maximum device temperature

A few preliminary studies have been made to see whether aspect ratio [$A = L/W$] has any effect on the peak temperature assumed by the L-corner. It is noticed that aspect ratio hardly influences the results of the present problem as long as convection is present in conjunction with radiation. When once convection is dispensed with and surface radiation alone is taken into reckoning, aspect ratio starts showing its effect on the peak device temperature (T_{max}). To elucidate the above, a study is made for $q_v = 10^6$ W/m^3 and $k_s = 0.25$ W/m K as shown in Fig. 10 by forcing the value of h to 0 W/m^2 K. The maximum temperature of the device (T_{max}) is found as a function of aspect ratio (A) for three typical surface emissivities ($\varepsilon = 0.45$, 0.65 and 0.85). The figure shows that, for a given aspect ratio, there is an expected drop in T_{max} with increasing ε owing to enhanced radiation activity. It may also be seen that, for a given emissivity, T_{max} decreases with increasing aspect ratio, more markedly for smaller values of A and less significantly towards larger values of A. The reason for the above could be attributed to decreasing length of the bottom leg of the L-corner with increasing aspect ratio. As the length of the bottom leg (W) decreases, the surface area of the device exposed to the ambient decreases. In the first sight, this may force one to think that the peak temperature of the device would shoot up. However, this does not happen because the present study has considered very small values of k_s [of the order of 1 W/m K]. Thus, an increase in the length of the bottom leg hardly brings any appreciable increment in the rate of heat dissipation. On the other hand, a decreasing W transforms the L-corner into a vertical plate [sans bottom leg]. The above exposes all the possible heat

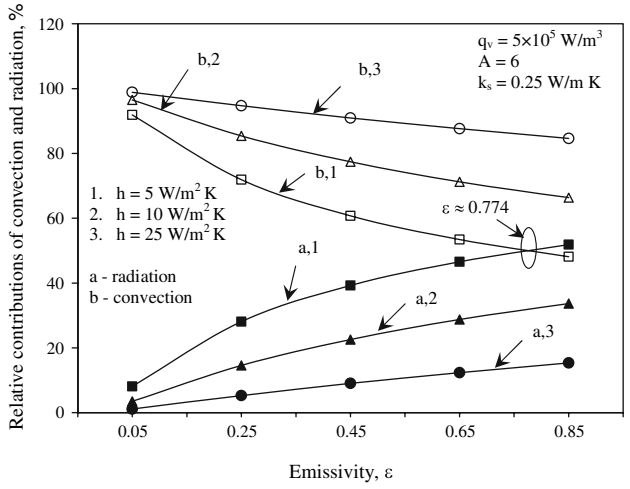

Fig. 9 Effect of surface emissivity on contributory roles of convection and radiation in heat dissipation from the device in different regimes of convection

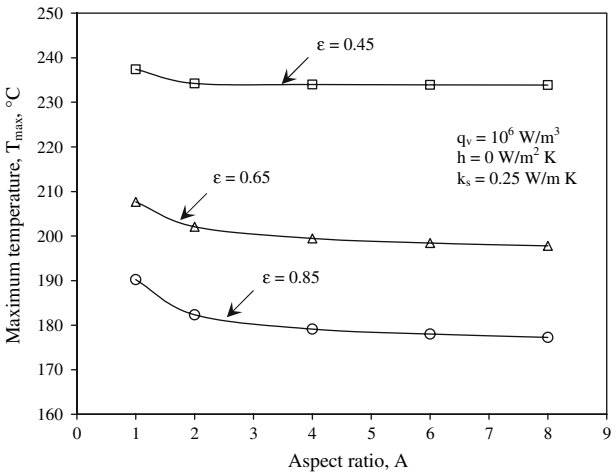

Fig. 10 Variation of maximum temperature of the L-corner with aspect ratio for three typical surface emissivities

transfer area of the device to the ambient with view factors from all the elements of the left leg of the L-corner tending to unity. The above obviously results in enhanced radiation dissipation from the device, which brings down the peak temperature. Obviously, the trend would have been different had the thermal conductivity of the L-corner been taken larger. In the present example, for $\varepsilon = 0.85$, T_{max} comes down substantially from 190.24 to 179.13°C as A increases from 1 to 4, while it further comes down only to 177.26°C for a subsequent increase in A from 4 to 8.

5 Concluding remarks

A numerical probe into the problem of multi-mode heat transfer from an L-corner equipped with three identical discrete heat sources has been made. The study considered interplay between heat generation, conduction, convection and radiation in deciding the temperature distribution along and heat dissipation from the L-corner. A finite-difference formulation has been used to discretise the governing non-linear partial differential equations. A computer code has been specifically written for solving the problem. The code has been tested for energy balance and an asymptotic validation has been made. An optimum grid system is obtained based on a detailed grid sensitivity analysis. The local temperature distribution along the L-corner, the peak temperature of the L-corner and the contributory roles played by convection and radiation are studied with reference to pertinent governing parameters. In addition to explicitly bringing out the effects of convection heat transfer coefficient (h) and surface emissivity (ε) on the results of the problem, an implicit attempt has been made to present representative optimum values for h and ε. The results of the study underline the necessity of taking surface radiation into reckoning in this kind of problems making use of gaseous cooling agents.

References

1. Zinnes AE (1970) The coupling of conduction with laminar natural convection from a vertical flat plate with arbitrary surface heating. ASME J Heat Transf 92:528–534
2. Tewari SS, Jaluria Y (1990) Mixed convection heat transfer from thermal sources mounted on horizontal and vertical surfaces. ASME J Heat Transf 112:975–987
3. Merkin JH, Pop I (1996) Conjugate free convection on a vertical surface. Int J Heat Mass Transf 39:1527–1534
4. Cole KD (1997) Conjugate heat transfer from a small heated strip. Int J Heat Mass Transf 40:2709–2719
5. Hossain MA, Takhar HS (1996) Radiation effect on mixed convection along a vertical plate with uniform surface temperature. Int J Heat Mass Transf/Waerme-und Stoffuebertragung 31:243–248
6. Gururaja Rao C, Balaji C, Venkateshan SP (2001) Conjugate mixed convection with surface radiation from a vertical plate with discrete heat source. ASME J Heat Transf 123:698–702
7. Gururaja Rao C, Balaji C, Venkateshan SP (2003) Conjugate mixed convection with surface radiation in a vertical channel with symmetric and uniform wall heat generation. Int J Trans Phenomena 5:75–101
8. Gururaja Rao C, Balaji C, Venkateshan SP (2002) Effect of surface radiation on conjugate mixed convection in a vertical channel with a discrete heat source in each wall. Int J Heat Mass Transf 45:3331–3347
9. Gururaja Rao C (2004) Buoyancy-aided mixed convection with conduction and surface radiation from a vertical electronic board with a traversable discrete heat source. Numerical Heat Transf A 45:935–956
10. Gururaja Rao C, Venkata Krishna A, Naga Srinivas P (2005) Simulation studies on multi-mode heat transfer from a square-shaped electronic device with multiple discrete heat sources. Numerical Heat Transf A 48:427–446
11. Gururaja Rao C, Nagabhushana Rao V, Krishna Das C (2008) Simulation studies on multi-mode heat transfer from an open cavity with a flush-mounted discrete heat source. Int J Heat Mass Transf 44:727–737
12. Sawant SM, Gururaja Rao C (2008) Conjugate mixed convection with surface radiation from a vertical electronic board with multiple discrete heat sources. Heat and Mass Transf (Published Online)
13. Peterson GP, Ortega A (1990) Thermal control of electronics equipment and devices. In: Hartnett JP, Irvine TF Jr (eds) Advances in heat transfer, vol 20. Academic Press Inc., San Diego, pp 181–314